Eur. Phys. J. B **35**, 357–364 (2003)
DOI: 10.1140/epjb/e2003-00288-x

THE EUROPEAN PHYSICAL JOURNAL B

Electron spin resonance studies on quantum tunneling in spinel ferrite nanoparticles

C.T. Hsieh and J.T. Lue[a]

Department of Physics, National Tsing Hua University, Hsin Chu 300, Taiwan

Received 12 May 2003 / Received in final form 29 August 2003
Published online 15 October 2003 –

Abstract. The electron spin resonance (ESR) spectrometer, a very sensitive instrument with fast detecting window to explore quantum phase transitions for magnetic nanoparticles, was exploited to study the fascinating interplay between thermal and quantum fluctuations in the vicinity of a quantum critical point. We have measured ESR in ferrofluid samples containing nanosize particles of Fe_2O_3. The evolution of the ESR spectrum with temperature suggests that quantum tunneling of spins occurs in single domain magnetic particles in the low temperature regime. The effects of various microwave fields, particle sizes, and temperatures on the magnetic states of single domain spinel ferrite nanoparticles are investigated. We can consistently explain experimental data assuming that, as the temperature decreases, the spectrum changes from superparamagnetic (SPR) to blocked SPR and finally evolves quantum superparamagnetic behaviour as the temperature lowers down further. A nanoparticle system of a highly anisotropic magnetic material can be qualitatively specified by a simple quantum spin model, or by the Heisenberg model with strong easy-plane anisotropy.

PACS. 76.30.-v Electron paramagnetic resonance and relaxation – 75.40.Cx Static properties (order parameter, static susceptibility, heat capacities, critical exponents, etc.) – 05.30.-d Quantum statistical mechanics – 75.50.Dd Nonmetallic ferromagnetic materials

1 Introduction

A quantum phase transition can differ fundamentally from a classical thermal transition because of its non-analyticity in the ground state energy of the infinite lattice system [1]. Unusual electronic and magnetic characteristics are prevalent at nonzero temperatures such as the metal-insulator transition in transition-metal oxides [2], non Fermi-liquid behavior of highly correlated f-electron compounds [3,4], abnormal symmetry states of high-T_c superconducting cuprates [5–8], and novel bistability of semiconductor heterostructures. The investigation of the remarkable properties of these systems attracts great efforts of researchers in condensed matter physics. The physics underlying the quantum phase transitions described above is quite involved and in many cases, has not been completely understood so far. In the high-T_c superconductors, for example, the superconductivity gives a direct way to study the quantum order-disorder transition. In heavy-Fermion materials, the characterization of the magnetic instability at $T = 0$ is complicated due to the presence of charge carriers and substitutional disorder. In spin glasses [9], one can vary the strength of quantum fluctuations to tune the spin glass phase into the paramagnetic phase.

Spin glasses [10,11] consist of random magnetic spins and random lattice sites in a material. Single magnetic domain nanoparticles, with a very high surface to volume ratio, exhibit strong frustration and disorder in the surface spins. A surface spin-glass layer is proved to be ubiquitous in magnetic nanoparticles at low temperatures [12,13]. The strong surface anisotropic field provides channels for quantum tunneling (QT) between spin-glass and quantum paramagnet. Macroscopic quantum tunneling of the magnetization [14] in single domain particles has been suggested to explain a plateau in the magnetic viscosity at low temperatures in particular systems such as $Tb_{0.5}Ce_{0.5}Fe_2$ [15], $CoFe_2O_4$ [16], FeC [17], and $NiFe_2O_4$ [18]. The low temperature magnetic viscosity of these systems shows a constant value below a finite temperature reflecting the independence of thermally over-barrier transitions and is the signature of quantum tunneling of the magnetization. Although there are some related evidences [15–18] about our results, we provide an alternative theory and experimental tool to survey analytically.

In this work, electron spin resonance (ESR) spectrometry is exploited to study the magnetic states of single

[a] e-mail: jtlue@phys.nthu.edu.tw

domain spinel ferrite nanoparticles. As the temperature decreases, the spectrum changes from superparamagnetic resonance (SPR) to blocked SPR and arrives at quantum SPR as the temperature lowers down further. A nanoparticle system of a highly anisotropic magnet can be qualitatively specified by a simple quantum spin model, or the Heisenberg model with strong easy-plane anisotropy [19]. Disordered spin-glass-like nanoparticles [12,13] become quantum paramagnets under anisotropy-assisted quantum tunneling. We tacitly assumed that an alternative approach would lead to a better understanding of the fascinating interplay in the vicinity of the quantum critical point in magnetic nanoparticles.

2 Theory

The Hamiltonian [19] of the Heisenberg model with strong easy-plane anisotropy with internal transverse fields σ_i^x without applying an external field is given by

$$H = -\sum_{i,j}^{N} J_{ij}\sigma_i\sigma_j - \Gamma\sum_{i}^{N}(\sigma_i^x)^2, \qquad (1)$$

where σ's are the Pauli spin matrices, $J_{ij} > 0$ are the longitudinal exchange couplings and Γ is the transverse anisotropy parameter for the spin-spin interaction causing quantum tunneling. Long-range force dominates the system for $J_{ij} \gg \Gamma$. We can express $H = H_0 + H_1$, where H_0 and H_1 correspond, respectively, to the first and second terms in the right hand side of equation (1), and commute with each other. The ground state of H_0 is long-range magnetically ordered and prefers ferromagnetism at low temperatures, while the ground state of H_1 favors the quantum paramagnetism. As the particle size decreases, the anisotropic field Γ increases up to a critical value [20,21], upon which a point of non-analyticity in the ground state energy is generated. The ground state of the total system varies from the magnetic long-range-order ground state H_0 to the paramagnetic ground state H_1. This means that the ground state energy is not continuous across the critical point at $T = 0$. But many experiments demonstrated that at some nonzero temperatures, though very low, an interplay between quantum and thermal fluctuations occurs.

In the case of applying an external transverse field, we consider the corresponding Hamiltonian in the same Heisenberg model [22] as

$$H = -\sum_{i,j}^{N} J_{ij}\sigma_i\sigma_j - \Gamma'\sum_{i}^{N}\sigma_i^x. \qquad (2)$$

The ground state of the first term prefers that the spins on neighboring ions are parallel to each other and become ferromagnetic for $J_{ij} \gg \Gamma$, whereas the second term allows quantum tunneling between the spin up $|\uparrow\rangle_j$ and spin down $|\downarrow\rangle_j$ states with amplitudes being proportional to the transverse field Γ'. Both the off-diagonal terms σ_i^x in equations (1) and (2) flip the orientation of the spin on a site by quantum tunneling. There can be a level-crossing field where an excited state becomes the ground state at the critical field and creates a point of nonanalyticity of the ground state energy as a function of Γ'. The second-order quantum phase transition usually occurs at the physically inaccessible $T = 0$ where it freezes into a fluctuationless ground state. The transverse critical field emanating a quantum phase transition occurring at $T > 0$ is smaller than the critical value Γ_c for $T = 0$ which decreases as the particle sizes reduce.

3 Sample preparation methods

Magnetic nanoparticles were prepared by co-precipitation method as conventionally implemented to make ferrofluids in the past [23]. A mixture of 2 g of hydrated ferrous chloride ($FeCl_2 \cdot 4H_2O$) and 5.4 g of hydrated ferric chloride ($FeCl_3 \cdot 6H_2O$) was dissolved in 300 c.c. of hot water, in which a solution of 5 g of sodium hydroxide was added with constant stirring. Black Fe_3O_4 particles were precipitated in water with a little remnant of sodium hydroxide. By adding oil acid and heating, Fe_3O_4 nanoparticles surrounded by surfactant were aggregated after adding hydrochloric acid. Washing the precipitation with water and then adding a solvent such as cyclohexane, the ferrofluid is finally produced. Other spinel ferrites can be prepared by replacing $FeCl_2$ by $NiSO_4$, $MnCl_2$, or $MgSO_4$. The ferrofluid of nanometer size looks apparently transparent. The shapes of most nanoparticles appear spherical, leading to non-demagnetization effect as examined by a transmission electron microscope (TEM).

The EPR experiment was performed by a continuous wave Bruker EMX-10 spectrometer operated at the X-band (9.46 GHz) at temperatures between 3.8 K and 400 K that is controlled by a flow-helium cryostat system with a stability of 0.1 K. A standard field modulation of frequency at 100 kHz and a phase sensitive detector was implemented to detect the field derivation of the absorbed power. The microwave absorption signal was recorded at a magnetic modulation field of 1.6 Oe at a microwave power of 0.8 to 20 mW. The samples were initially zero-field cooled at 3.8 K and then heated to measure the EPR spectra at different temperatures.

4 Results and discussion

At high temperatures, single domain magnetic nanoparticles are thermally free to orient their spin directions and exhibit superparamagnetic properties. The relaxation time τ_R depends on temperatures as [24]

$$\tau_{_R} = \tau_{_0}\exp(K_aV/k_{_B}T), \qquad (3)$$

where K_a is the magnetic anisotropy constant, V is the particle volume, and τ_0 is a typical time constant of the order $10^{-10} \sim 10^{-12}$ s [25,26]. Below the blocking temperature T_B, depending on a typical time scale

of measurements τ, the slow down of thermal motion implies the magnetic nanoparticles to undergo a transition from superparamagnetic to blocked SPR which behaves like a ferromagnetic state for the total system. The electron paramagnetic resonance experiment reveals that the anisotropy field decreases as the measuring temperature increases above the blocking temperature wherein $\tau_{_E} \sim 10^{-10}$ s. However, the zero-field-cooled magnetization measurement indicates that the super paramagnetic relaxation time is estimated to be $\tau_{_m} \sim 10^2$ s. Since the time scale for observing the ESR spectra is much shorter than that for magnetization measurements, the blocking temperature T_B^E for ESR is much higher than that of the magnetization measurements T_B^m. The ratio of the two blocking temperatures, with a prosaic manipulating of equation (3), is given by

$$\frac{T_B^E}{T_B^m} = \frac{\ln(\tau_{_m}/\tau_0)}{\ln(\tau_{_E}/\tau_0)}. \tag{4}$$

Inserting the values of $\tau_{_E}$, $\tau_{_m}$, $T_B^E = 30$ K, and $T_B^m = 4.5$ K, we can estimate the τ_0 to be about 10^{-12} s which is in agreement with the results of other experiments [25,26]. Therefore the ESR provides an excellent method to detect the quantum phase transition at temperatures higher than $T = 0$.

The temperature dependent EPR spectra for Fe_3O_4 nanoparticles obtained from 220 K to 4 K are specified by curves as shown in Figure 1. The tiny spectrum centered at $g \sim 4.3$ is attributed to the isolated spin $^6S_{5/2}$ of the remnant Fe^{3+} ions when the second–order crystal field coefficient with axial symmetry vanishes while that with rhombic symmetry persists [27]. The relatively narrow SPR line (∼100 Gauss) fades and the broad blocked SPR resonance line (∼1500 Gauss) manifests as the temperature decreases to about 35 K. Since the anisotropic field H_a for Fe_3O_4 nanoparticles is fairly small (an order of 50 G), the SPR line is almost centered at the resonance magnetic field $H_0 = 3375$ G for free electron spins. This line position almost is not shifted as temperatures decrease on account of this small H_a. The linewidth reveals abnormal broadening (∼1500 Gauss) below the blocking temperature (63 K) and the broad line grows and becomes prevalent until the temperature reaches 22 K. The SPR line width depends on the domain size of particles and the anisotropic field. The narrowing of the SPR linewidth at high temperatures is attributed to the thermal fluctuations of the magnetic nanoparticles while the broadening of the blocked SPR results from the line up of the magnetizations of all particles that enhances the anisotropic field at low temperatures. At even lower temperatures wherein the quantum paramagnetic state is reached, the quantum tunneling of the surface spin glass largely reduces the domain size within each nanoparticle. The linwidth is very sharp in the QSP state.

As temperatures decrease to 20 K, there is a renascence of an anomalous paramagnetic resonance with a linewidth of about 60 Gauss at $g \sim 2$ with the amplitude growing and decaying until the temperature decreases to about 8 K. An anomalous paramagnetic resonance prevails

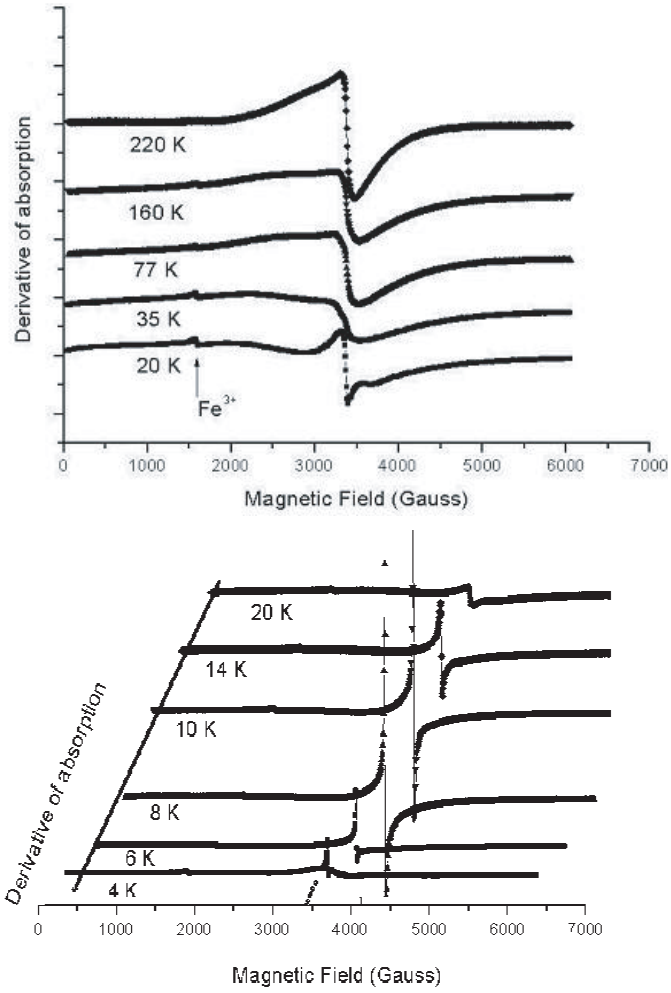

Fig. 1. The ESR spectra for Fe_3O_4 ferrofluid measured at various temperatures between 220 K and 4 K. The spectra below 20 K are canted to express the same resonance position without turbidity of signals.

behaving like a free exchange-coupled giant spin which largely reduces the linewidth to about 10 Gauss as expressed to be a quantum superparamagnetic state. The anisotropic field $K_\perp$ increases as temperature decreases resulting in a higher tunneling rate. The domain size of the quantum SP particle decreases attributing to prominent transfer of magnetic domains into surface spin glass state.

Considering that the strong surface anisotropic field would destroy the internal exchange force making the long-range ferromagnetic state to become paramagnetic can better elucidate this quantum paramagnetic state existing at low temperatures. Below 8 K, the amplitude of paramagnetic resonance decreases resulting from the commencement of maximizing the anisotropic field and the reducing of thermally assisted paramagnetic resonance.

The demagnetization vanishes in the case of spherical nanoparticles and in case of the anisotropic field being small comparing to the external field, the microwave

frequency at magnetic resonance may be evaluated as follows

$$\omega = \gamma\sqrt{(H_0 + H_a)(H_0 + H_a + H_d)}, \quad (5)$$

where γ is the gyromagnetic ratio, H_0 is the applied resonant field, H_a is the crystalline anisotropy field, and H_d is the demagnetization field. If the anisotropy is small compared to the Zeeman energy, the resonance condition can be approximated by the sum of external and anisotropy field, one can use the first order approximation of the angular dependence [27]. The intensity of the magnetic resonance spectrum at field H can be calculated as

$$I(H) \propto \iiint_{\vartheta\varphi d} L\left[H - (H_0 + H_a + H_d), W\right] \times P(r)\sin\vartheta dr d\vartheta d\varphi, \quad (6)$$

where $L[H - (H_0 + H_a + H_d), W]$ is a Gaussian or Lorentzian lineshape, W is the individual line width for a particle of a given size, and $P(r)$ is the particle size distribution assuming to be a log-normal-like [10]. Figure 2 reveals the simulated total spectrum for mixed nanoparticles with the most probable particle size of 3.8 nm with a distribution range of 0.74 nm. The inset of Figure 2 shows that the line width sharply broadens as the particle size increases from 1 nm to 3 nm. The small nanoparticles contributing to the SPR have a line width of about 100 Gauss while large particles yield a board FMR-like line. This simulation clearly delineates the SPR linewidth strongly depending on the sizes of nanoparticles. The narrowing factor f of the line width due to thermal motion is estimated to be $f = \tau_{sp}/\tau_L \approx M_s H_0 \exp(K_a V/k_B T)/\gamma_0$, where M_s is the magnitization of a single particle, τ_{sp} is the thermal fluctuation time, τ_L is the Larmor precession time, and γ_0 is the gyro-magnetic ratio. Hence, the linewidth of superparamagnetic resonance ($f \ll 1$) should be proportional to the exponent of the particle volume V.

Figure 3 portraits the occurrence of the amplitude peak at low temperatures and the linewidth variations for super paramagnetic, ferrimagnetic, and quantum paramagnetic resonance, which are about 100 G, 1500 G, and 10 G respectively. The spin susceptibility which is proportional to the integration of the intensity is hidden in the very broad spectrum line at low temperatures. The line width of the paramagnetic resonance signal arising from quantum fluctuations is independent of temperatures. The demarcation illustrates that the emergence of the interplay between quantum and thermal fluctuations, magnetic long-range order, and superparamagnets, respectively, occurs at temperatures from 4 K to 22 K, from 22 K to 63 K and above 63 K. Two prominent critical points associated with the classically thermally driven from SPR to blocked SPR and the quantum tunneling from magnetic long-range order to quantum paramagnet are appraised. The sharply narrowing down of the linewidth for quantum SPR may be attributed to largely reducing of the domain size by quantum tunneling yielding the same result as Figure 2. The amplitude of the quantum paramagnetic

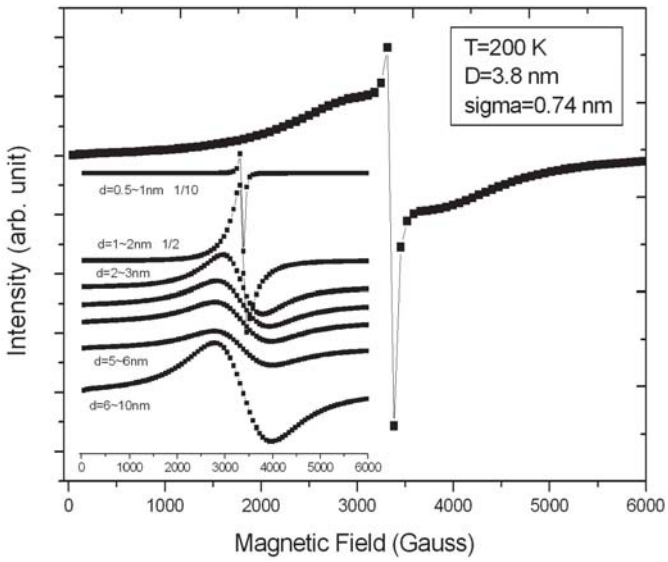

Fig. 2. The simulated SPR spectra for various particle sizes. The main curve is the combined spectrum for a log-Gaussian distribution of particle sizes at the most probable size of 3.8 nm with a width of 0.74 nm while the inset represents subtle curves for various particle sizes. The reduction factor of the signal amplitude is indicated following the size.

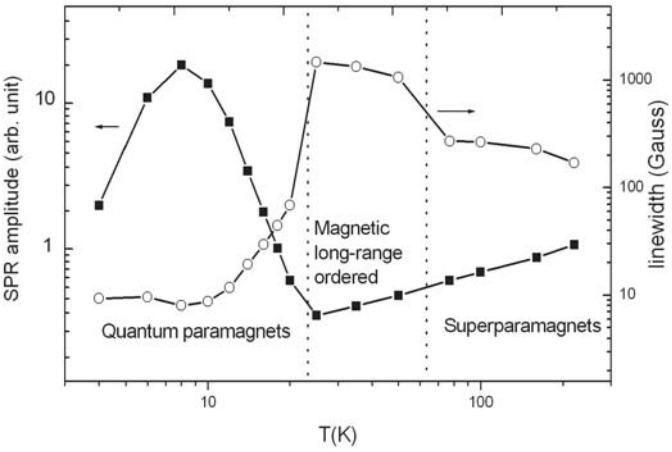

Fig. 3. The ESR line widths and amplitudes at various temperatures for Fe_2O_3 ferrofluid are displayed to specify three magnetic states.

resonance increases to a maximum value at 8 K as the temperature decreases which is different from the appearance of the line width. The amplitude reaches to maximum due to thermal fluctuations in the quantum critical point at 8 K.

The temperature dependence of the quantum paramagnetic spin susceptibility of Fe_3O_4 nanoparticles which is proportional to the double integral of the field derivative of the absorption curve, is plotted in Figure 4. Finite temperatures spanning across the quantum critical region is controvertible. The inset of Figure 4 indicates the log-to-log plot of spin susceptibility χ versus t within the critical region. The best fitting of the critical exponent obtained for the simple power law dependence $\chi \propto t^{-\gamma}$, where t is

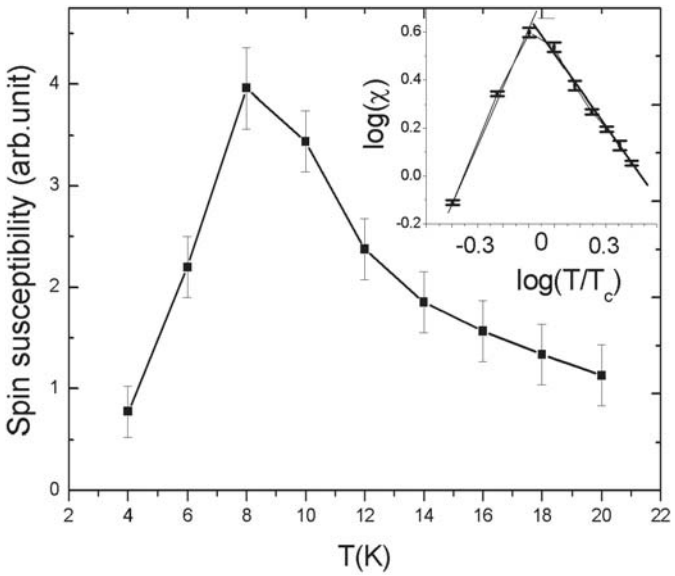

Fig. 4. The spin susceptibility (the double integral of the field derivative curve) Fe_3O_4 ferrofluid at various temperatures, the inset is the log-log plot of the static spin susceptibility versus the reduced temperature $t = T/T_c$ which reveals a peak at $log(t) = 0$. The slopes are estimated to be about 1.7 and 2.3 in the low and high temperature regions, respectively. The spin susceptibility is taken the double integration between 3300 G $\sim$ 3450 G of the QPR parts so that the data points are different with Figure 3.

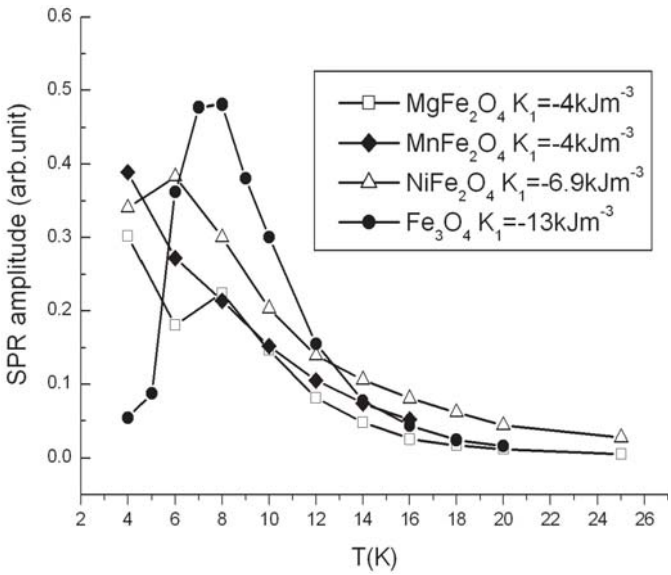

Fig. 5. The amplitude of superparamagnetic resonance for various spinel ferrites which are characterized by different anisotropy fields.

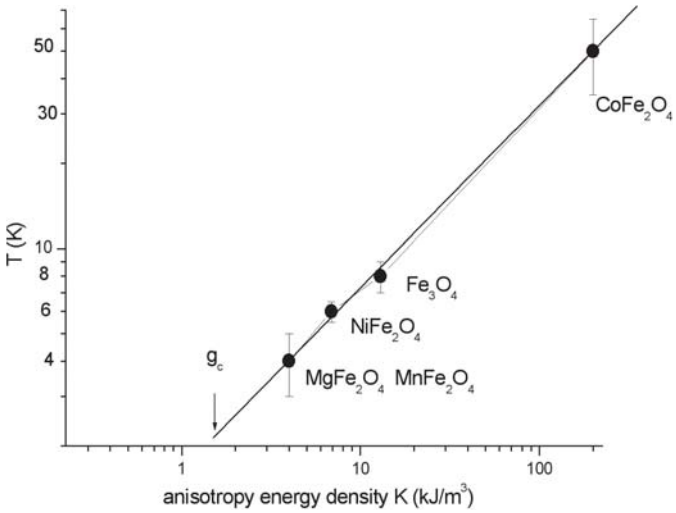

Fig. 6. The cross-over temperature for blocked SPR to quantum superparamagnetic resonance (QSP) increases with the anisotropic constant for various ferrites.

the reduced temperature T/T_c for the paramagnetic state, implies $\gamma \approx 2.3 \pm 0.2$ on the low temperature side, and $\gamma \approx 1.7 \pm 0.2$ on the high temperature side, respectively. Figure 5 shows the amplitudes of quantum paramagnetic resonance spectra for various spinel ferrite nanoparticles. We have prepared four spinel ferrites with different crystalline anisotropy. The corresponding linewidths are about 550 Gauss, 25 Gauss, and 35 Gauss with respect to $MnFe_2O_4$, $MgFe_2O_4$, and $NiFe_2O_4$ nanoparticles. The critical temperature increases with the crystalline anisotropy that is in accord with the Heisenberg model with strong easy-plane anisotropy. Apparently, we found that Fe_3O_4 nanoparticles which have a higher crystalline anisotropy field ($K_a = -13$ kJm^{-3}) exhibit the QT at higher temperature $\sim$8 K, while the spinel ferrites $NiFe_2O_4$ (or $MgFe_2O_4$), and $MnFe_2O_4$ which have $K_a = -6.9$ kJm^{-3} and $K_a = -4$ kJm^{-3} respectively, have $T_c \sim 6$ K and $T_c < 4$ K. We clearly demonstrate that the low temperature paramagnetic resonance spectrum is indeed anisotropic field dependent and agrees with the theory. The cross-over temperature for blocked SPR to quantum superparamagnetic resonance increases with the anisotropic constant as shown in Figure 6.

In presence of transverse magnetic field, the Heisenberg model presumes the occurrence of QT. This transverse field includes the inherited internal anisotropic field and the external applied microwave field. As the total transverse field exceeds the critical value, the second term of the Hamiltonian in equation (2) allows the quantum tunneling between the down spin $|\downarrow\rangle_j$ and up spin $|\uparrow\rangle_j$ states. Figure 7 delineates the SPR amplitudes of Fe_3O_4 nanoparticles increasing with transverse microwave fields. The inset shows that the critical temperature increases with the microwave field. The occurrence of lowering down the critical temperature as the microwave field decreases alluding the evidence of the quantum tunneling nature where the transverse magnetic field H reduces the barrier energy for quantum tunneling as given by [14]

$$U = K(1 - H/H_c)^2, \tag{7}$$

where $H_c = 2\ K/M_0$, M_0 is the magnetic moment per unit volume of the material.

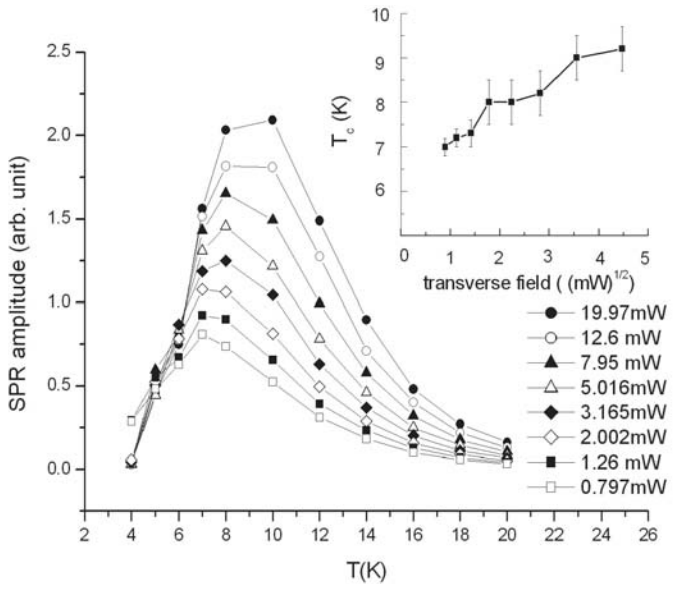

Fig. 7. The amplitude of SPR signal of Fe_3O_4 with different transverse microwave magnetic fields. The inset shows an increase of the critical temperatures on various transverse fields where a nonzero interception of T_c at zero applied field implies that the internal anisotropy field dominates QPT.

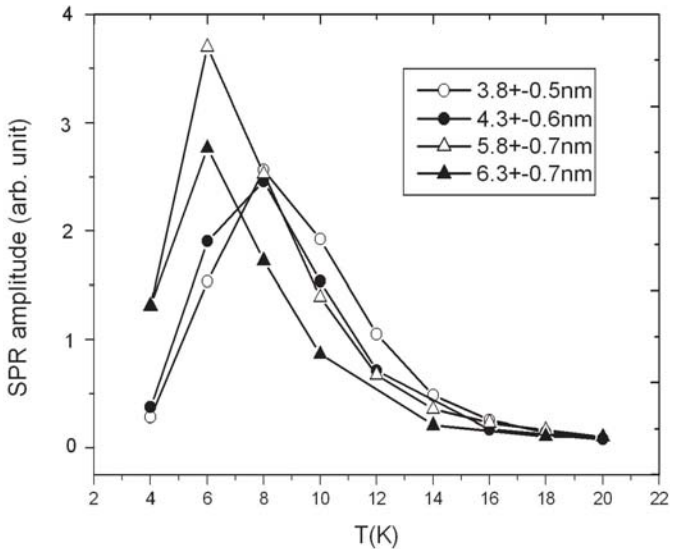

Fig. 8. The critical temperature of QPT decreases as the size of Fe_3O_4 nanoparticles increases.

The size dependence on quantum paramagnetic amplitudes in magnetite nanoparticles is depicted in Figure 8. To include the large surface anisotropic field for nanoparticles, the anisotropic energy ΔE_a of the observed magnetization relaxation rate as dictated in equation (3) should be replaced by $\Delta E_a = K_{eff}V = K_aV + K_sS$, where $V = \frac{4\pi}{3}(d/2)^3$, $S = 4\pi(d/2)^2$, K_a and K_s are the volume and surface anisotropic constant, respectively. We can apparently obtain that the effective anisotropic energy density is inversely proportional to the size of the nanoparticle as

$$K_{eff} = K_a + \frac{6}{d}K_s. \tag{8}$$

Previous works [20,21] denoted that the anisotropic field for magnetic nanoparticles is enhanced by two or three orders of magnitude over that of bulk values. Accordingly, this experiment illustrates that for magnetite with particle size of 10 nm, no QT was observed by any strong transverse field at temperatures above 4 K.

Finally we compare the ESR results to the magnetization measurements governed by apparently slower observing time scales. To justify the existence of SP, blocked SP and quantum SP states at various temperatures, we used the Co-ferrite nanopartiles which have a much larger anisotropic field. The magnetization for $CoFe_2O_4$ ferro fluid as a function of temperatures was measured by a MPMS2 superconducting quantum unit interference device (SQUID) as shown in Figure 9. Above T_B the particles are superparamagnetic where the field cooled (FC) and zero field cooled (ZFC) curves merge that elucidates the alignment of the anisotropic spins for the field cooled spectrum. Two remarkable transition points were denoted

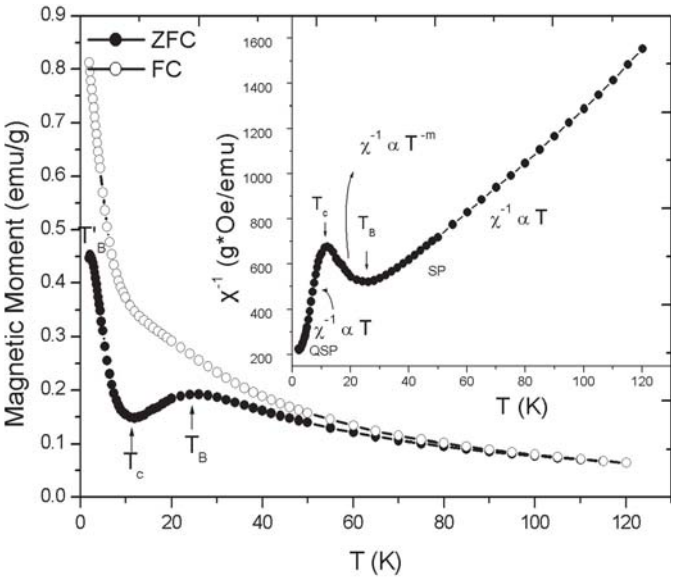

Fig. 9. Temperature dependence of the magnetization of $CoFe_2O_4$ measured in modes of FC at an external field of 10 G (open circles) and ZFC (closed circles). The inset illustrates the reciprocal susceptibility versus T. Two remarkable points, T_B, and T_c, indicate the transition from SP to blocked SP, and from blocked SP into quantum SP.

as T_B and T_c in the ZFC curve to represent the blocking state between 24 K and 11 K and the cross temperature at 11 K. Above T_B, the Co-ferrite nanoparticles exhibit superparamagnetism due to thermal fluctuations of the magnetic moments while blocked to the original ferrimagnetic order at temperatures below T_B. There was an unconventional increase of magnetization below T_c and seemed to be blocked again at 2.4 K. We have attributed the unconventional increase of magnetization below T_c to a quantum superparamagnetic state. The activated

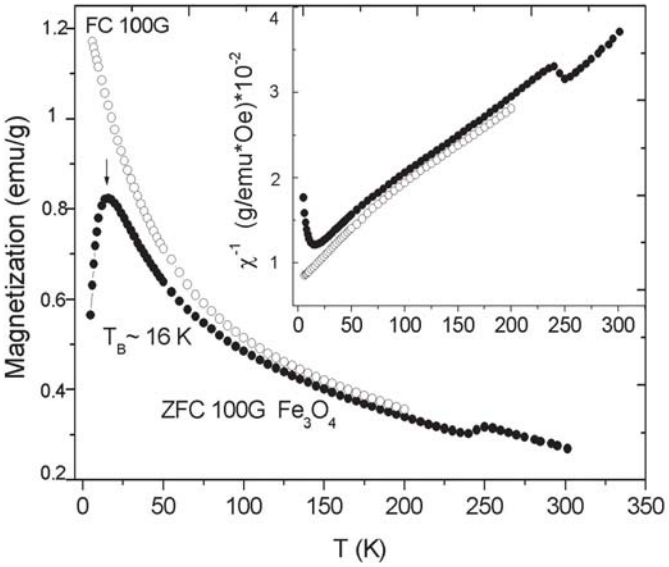

Fig. 10. The plot of the magnetization as a function of temperatures for the Fe_3O_4 ferrofluid. The empty and filled symbols represent the field cooled and zero-field cooled magnetizations, respectively.

energy of Co-ferrite nanoparticles at the blocking temperature is estimated to be $E_a \approx 30k_BT_B = K_aV$. With $K_a \sim 6 \times 10^6$ erg/cm^3 and $T_B \sim 24$ K, we can evaluate $V \sim 31.6$ nm^3, which corresponds to a particle diameter of ∼3.1 nm.

The reciprocal susceptibility χ^{-1} of Co-ferrite NPs is plotted in the inset of Figure 9. The magnetic susceptibility at temperatures between Q_{sp} and T_c and above T_B follows the Curie law. The susceptibility is inverse linearly proportional to the temperature. The slope of the curve is represented as the reciprocal of Curie constant C, where $C = Ng^2S(S+1)\mu_B^2/3k_B$. The Curie constant above the blocking temperature T_B is smaller than that of below T_C indicating that the number N of spins responsible for the Curie like behavior below T_C is clearly smaller than the N above T_B resulting from the main part of the spins is involved in the blocked state. So it is difficult to conclude about the increase or decrease of the effective spin (i.e. magnetic moment) from the inverse slope. However, in conjunction with the evidence of ESR measurement, it clearly demonstrates that the increasing magnetic moment is not due to thermal activation of small size components.

We have performed the SQUID measurement (Fig. 10) for Fe_3O_4 ferrofluid that has a rather low anisotropic field H_a to stimulate quantum tunneling. The transition temperature measured by SQUID for the SPR to FMR-like transition (near 14 K) is much lower than the result as appraised in Figure 3 owing to the much lower blocking temperature of SQUID than that of ESR. The small peak at 250 K is attributed to the liquid to solid phase change.

5 Conclusion

We have studied the ESR response of ferrofluid Fe_3O_4 samples as a function of temperatures. The experimental data can be consistently explained in the framework of a qualitative model of the evolution of the nanoparticle magnetic system with decreasing temperatures from the superparamagnetic, to blocked superparamagnetic and finally to the quantum tunneling regime. Size and anisotropy dependence of the transition temperature agree with the Heisenberg model with strong easy-plane anisotropy. The critical temperatures of the quantum superparamagnetic resonance spectra are also proportional to the intensity of transverse magnetic field in accord to the Heisenberg model in the external transverse field. Plausibility of a quantum phase transition might occur as a consequence of the critical exponent $\gamma = 1.7 \sim 2.3$. More evidences for clues of this eventual QT should be provided such as measurements of heat capacity and ac susceptibility. The possibility of QPT in magnetic nanoparticles is vital in theoretical and experimental point of view.

The authors are indebted to Professor T.M. Hong for his stimulated discussion. This work was supported from the National Science Council of the Republic of China under the contract N0.92-2112-M007-057 and the Ministry of Education under the contract 92-FA-04-AA.

References

1. J.A. Hertz, Phys. Rev. B **14**, 1165 (1976); M.A. Contentino, *ibid.* **47**, 11587 (1993); A.J. Millis, *ibid.* **48**, 7183 (1993)
2. S.A. Carter, T.F. Rosenbaum, J.M. Honig, J. Spalek, Phys. Rev. Lett. **67**, 3440 (1991); Phys. Rev. B **48**, 16841 (1993)
3. H.V. Lohneysen, T. Pietrus, G. Portisch, H.G. Schlager, A. Schroder, M. Sieck, T. Trappmann, Phys. Rev. Lett. **72**, 3262 (1994); B. Bogenberger, H.V. Lohneysen, *ibid.* **74**, 1016 (1995)
4. M.B. Maple, C.L. Seaman, D.A. Gajewski, Y. Dalichaouch, V.B. Barbetta, M.C. de Andrade, H.A. Mook, H.G. Lukefahr, O.O. Berna, D.E. MacLaughlin, J. Low. Temp. Phys. **99**, 223 (1995)
5. S. Chakravarty, B.I. Halperin, D.R. Nelson, Phys. Rev. B **39**, 2344 (1989)
6. S. Sachdev, J.Ye, Phys. Rev. Lett. **69**, 2411 (1992)
7. B. Keimer, R.J. Birgeneau, A. Cassanho, Y. Endoh, R.W. Erwin, M.A. Kastner, G. Shirane, Phys. Rev. Lett. **67**, 1930 (1991)
8. L.Y. Chen, J.T. Lue, R.S. Liu, Phys. Rev. B **52**, 12883 (1995)
9. J. Miller, D.A. Huse, Phys. Rev. Lett. **70**, 3147 (1993)
10. J.T. Lue, W.C. Huang, S.K. Ma, Phys. Rev. B **51**, 14570 (1995)
11. W.C. Huang, J.T. Lue, Phys. Rev. B **59**, 69 (1999)
12. R.H. Kodama, A.E. Berkowitz, E.J. McNiff, Jr. S. Foner, Phys. Rev. Lett. **77**, 394 (1996)
13. B. Martinez, X. Obradors, Ll. Balcells, A. Rouanet, C. Monty, Phys. Rev. Lett. **80**, 181 (1998)
14. E.M. Chudnovsky, J. Tejada, *Macroscopic Quantum Tunneling of the Magnetic Moment* (Cambridge, 1998), p. 94

15. C. Paulsen, L.C. Sampaio, R. Tachoueres, B. Barbara, D. Fruchart, A. Marchand, J.L. Tholence, M. Uehara, J. Magn. Magn. Mater. **116**, 67 (1992)
16. X.X. Zhang, J.M. Hernandez, J. Tejada, R.F. Ziolo Phys. Rev. B **54**, 4101 (1996)
17. J. Tejada, L. Balcells, S. Linderoth, R. Perzynski, B. Barbara, J.C. Bacri, J. Appl. Phys. **73**, 6952 (1993)
18. R.H. Kodama, C.L. Seaman, A.E. Berkowitz, M.B. Maple, J. Appl. Phys. **75**, 5639 (1994)
19. V. Yu. Irkhin, A.A. Katanin, Phys. Rev. B **58**, 5509 (1998); C.T. Hsieh, J.T. Lue, Phys. Lett. A **300**, 636 (2002), ibid. **316**, 329 (2003)
20. A. Garvin, C.L. Chien, J. Appl. Phys. **67**, 938 (1990)
21. G. Xiao, S.H. Liou, A. Levy, J.N. Taylor, C.L. Chien, Phys. Rev. B **34**, 7573 (1986)
22. S. Sachdev, *Quantum Phase Transitions* (Cambridge, 1999), p. 8
23. H.J. Williams, R.M. Bozorth, W. Shockley, Phys. Rev. **75**, 155 (1949)
24. L. Néel, Ann. Geophys. **5**, 99 (1949)
25. C. Johansson, M. Hanson, P.V. Hendriksen, S. Morup, J. Magn. Magn. Mater. **122**, 125 (1993)
26. D.P.E. Dickson, N.M.K. Reid, C. Hunt, H.D. Williams, M. El-Hilo, K. O'Grady, J. Magn. Magn. Mater. **125**, 345 (1993)
27. V.K. Sharma, A. Baiker, J. Chem. Phys. **75**, 5596 (1981); C.T. Hseih, W.L. Huang, J.T. Lue, J. Phys. Chem. Solids **63**, 733 (2002)
28. R.S. de Biasi, T.C. Devezas, J. Appl. Phys. **49**, 2466 (1978)
29. R. Berger, J. Kliava, J.C. Bissey, V. Baietto, J. Appl. Phys. **87**, 7389 (2000)